Investigations into modifications of neuromuscular physiology by axonal transport disruptions in *Drosophila* SOD1 mutants

Tristan C. D. G. O'Harrow[1]*, Atsushi Ueda[1]*, Xiaomin Xing[1]*‡, Chun-Fang Wu[1]

[1] Department of Biology, University of Iowa, Iowa City, IA 52242, USA

* Equal contribution

‡ Current address: Department of Pharmacology, School of Medicine, University of California, Davis, CA, 95616

Abstract

Cu/Zn superoxide dismutase (SOD1) is a cytoplasmic antioxidant enzyme, which, when mutant in humans, is linked to familial cases of the motor neurodegenerative disease amyotrophic lateral sclerosis (ALS). The *Drosophila* SOD1 gene (*Sod*) shares a highly conserved sequence with the human homolog, and this study includes examinations of the established hypomorphic *n108* allele (Sod^{n108}), alongside a knock-in construct of the *G85R* allele found in human ALS patients (Sod^{G85R}). In addition to previously documented decreased adult lifespan and attenuated motor function, we show that *Sod* mutant *Drosophila* display high mortality rates during larval and pupal development. Immunostaining of neuronal membrane at neuromuscular synapses in *Sod* mutant larvae revealed presynaptic terminals of abnormal, swollen morphology. In Sod^{G85R} larvae, *in vivo* mitochondrial staining demonstrated the presence of aggregated mitochondria inside the swollen synaptic terminals, and a genetically encoded GFP construct targeted to mitochondria revealed aggregates of mitochondria inside the axon bundles of Sod^{G85R} larvae. In whole-cell recordings of neuromuscular transmission, both Sod^{n108} and Sod^{G85R} exhibited

lower muscle input resistance and smaller miniature excitatory junction potentials (mEJPs) compared to WT. However, evoked EJPs were similar to those of WT. Focal electrophysiological recording showed that both *Sod*^{n108} and *Sod*^{G85R} NMJ terminals displayed slightly higher release probability than WT terminals. Treatment of *Sod*^{G85R} with the *Shaker* channel (Kv1) blocker 4-aminopyridine (4-AP) and the broad-spectrum K^+ channel blocker tetraethylammonium (TEA) induced prolonged "plateau-like" potentials at the larval NMJ upon electrical stimulation. Altogether, this study provides a snapshot of the alterations in mitochondrial distribution, synaptic morphology, and neurotransmission that characterize the motor neurons of *Sod* mutants prior to neurodegeneration and death of the organism.

Introduction

The generation of reactive oxygen species (ROS) is a ubiquitous feature of energy metabolism in living cells. ROS are a class of oxygen-containing molecules that readily oxidize other molecules upon contact, and as a result can cause a significant amount of damage to cellular components over time (Lushchak, 2014). To mitigate this effect, a broad variety of eukaryotic and prokaryotic organisms produce antioxidant enzymes to maintain oxidative homeostasis (Matés et al., 1999). While ROS are produced endogenously as byproducts of metabolic processes, including mitochondrial oxidative phosphorylation, they can also be generated from exogenous sources like toxins, drugs, and pollutants (Chen et al., 2003; Ali et al., 1996; Block & Calderón-Garcidueñas, 2009). The disruption of oxidative homeostasis that occurs as a result of increased ROS load or a decrease in antioxidant activity is termed 'oxidative stress' (Sies, 1997).

The accumulation of oxidative damage due to oxidative stress over time is considered a normal part of aging in macroorganisms, and ROS have been implicated as signaling molecules in healthy physiological processes ranging from cell differentiation to synaptic plasticity (Thannickal & Fanburg, 2000; Massaad & Klann, 2011). However, under increased oxidative stress, cellular proteins are more prone to misfolding, lipids to peroxidation, and nucleic acids to breakage and mutation (Berlett & Stadtman, 1997; Altan et al. 2003; Aitken & Krausz, 2001). Possibly as a result of these effects, increased oxidative stress has been implicated in neurodegenerative diseases, cardiovascular diseases, and cancer (Liguori et al., 2018; Uttara et al., 2009; Dhalla et al., 2000; Sosa et al.,2013).

Molecular species considered ROS include both free radicals such as the superoxide (O_2^-), the peroxide O_2^{-2}, and the hydroxyl OH^-, and molecules without unpaired valence electrons, such as hydrogen peroxide (H_2O_2) and the hydroxyl OH (Lushchak, 2014). Cells express a variety of antioxidant enzymes to neutralize these ROS and their derivatives. These enzymes include catalase, glutathione peroxidases, and superoxide dismutases (Matés et al., 1999). Evidence suggests that production of antioxidant enzymes may be generally downregulated in aged organisms, so the contributions of oxidative stress to the aging process may include not just oxidative damage accumulated over the lifespan, but also damage from increased oxidative stress later in the lifespan (Baek et al, 2016).

The antioxidant enzyme Cu/Zn superoxide dismutase (SOD1) behaves as a protein homodimer that mainly localizes to the cytosol, and specifically targets superoxide molecules (O_2^-) for neutralization (Perry et al., 2010; Culotta & Daly, 2013; Mondola et al., 2016). As SOD1 interacts with O_2^- , the enzyme alternates between reducing Cu^{2+} to oxidize O_2^- to molecular oxygen (O_2), and oxidizing Cu^+ and donating protons to reduce O_2^- to H_2O_2

(Mondola et al., 2016; Perry et al., 2010). H_2O_2 produced by this process is then converted by the enzyme catalase into molecular oxygen and water (O_2 & H_2O) (Mondola et al., 2016).

The gene encoding SOD1 (*Sod*) is highly conserved across a wide range of species, including humans, mice, the worm *Caenorhabditis elegans* (*C. elegans*), and the fruit fly *Drosophila melanogaster*. The functionally null *n108* allele of the *Drosophila* gene for SOD1 (*Sod*) was generated by exposure of *Drosophila* to the mutagen ethyl methanesulfonate (Campbell et al., 1985). Flies homozygous for the *n108* allele display hypersensitivity to paraquat (Pq^{2+}), a toxin that induces acute oxidative stress (Phillips et al., 1989). All Sod^{n108} flies in a cohort died when exposed to an aqueous solution containing 5 mM Pq^{2+} for 48 hrs, whereas over 80% of control flies survived in identical conditions (Phillips et al., 1989). Even without exposure to toxins, Sod^{n108} confers a reduced adult lifespan, with fewer than 5% of Sod^{n108} flies living longer than 20 d., compared to lifespans longer than 50 d. for over 70% of flies in control cohorts.

In contrast, *C. elegans* that lack activity not just of their homolog of SOD1, but lack the activity of all five SOD genes present in wild-type *C. elegans*, have a wild-type lifespan under normal conditions, though they display increased sensitivity to pharmacologically-induced oxidative stress (Van Raamsdonk & Hekimi, 2012). Mice null for their SOD1 gene have a mean lifespan ~87% as long as that of their wild-type counterparts, a phenotype less striking than the *Drosophila* lifespan phenotype (Zhang et al., 2016). The disparities between the percent decreases in lifespan of SOD1 null mutants of different species suggest that, while principal enzymatic functions appear to be evolutionarily conserved, the relative importance of SOD1 in general organismal physiology or additional functions of the protein may be more divergent. One such additional SOD1 function has been observed in yeast, where, under elevated oxidative stress, the protein relocates to the nucleus. Association of SOD1 with

103 promoters in the yeast nucleus suggests that it regulates expression of 'oxidative response'
104 genes (Tsang et al., 2015). Some human patients with the neurodegenerative disease
105 amyotrophic lateral sclerosis (ALS), popularly known as Lou Gehrig's disease or motor
106 neuron disease, have been found to carry mutations in the gene for SOD1, and can exhibit
107 decreased overall SOD1 activity (Rosen et al., 1993; Saccon et al., 2013).
108
109 ALS is a fatal neurodegenerative disease in which the gradual death of upper motor neurons
110 in the cortex and brainstem and of lower motor neurons in the spinal cord causes the
111 muscles they innervate to weaken and atrophy (Rosen et al., 1993; Rowland & Shneider,
112 2001). As a result, patients progressively lose the ability to walk, swallow, and breathe, with
113 an average life expectancy of three to five years after diagnosis (Galvin et al., 2017;
114 Hardiman et al, 2011). Approximately 2.7 in 100,000 people are affected by ALS across
115 Europe and North America, with an age of onset most commonly between 50 and 65 years
116 (Zarei et al., 2015). Precise causes for the development of ALS are still under study, but
117 research-supported risk factors include specific genetic mutations, as well as cigarette
118 smoking (Zarei et al., 2015). More controversially proposed risk factors include physical
119 activity and exposure to agricultural chemicals and electromagnetic fields (Zarei et al., 2015).
120 Also missing from current research are clear, early signs of ALS progression. The 5-10% of
121 ALS cases demonstrated to have a heritable genetic component are classified as familial
122 ALS (FALS), and the remaining 90-95% of cases are classified as sporadic ALS (SALS)
123 (Zarei et al., 2015). Mutations in the gene for SOD are the most commonly identifiable risk
124 factor for FALS, and other mutations found in FALS patients include mutations in the genes
125 for the nucleic acid-binding proteins TAR DNA-binding protein 43 (TDP-43), Fused in
126 sarcoma (FUS), and angiogenin (Zarei et al., 2015). While ALS is believed to involve
127 relatively-specific degeneration of motor neurons for reasons that remain unclear, the
128 disease has at times been observed to appear alongside frontotemporal dementia (FTD),

which involves non-motor neuron degeneration in the frontal and temporal lobes (Mackenzie & Rademakers, 2008).

Due to its central antioxidant function, dysfunction of SOD1 in an organism as a result of mutation results in an increase in oxidative stress. Extremely high oxidative stress can cause enough damage that cells die by necrosis, a disorderly form of cell death that does not follow from distinct signaling pathways (Tang et al., 2013). However, oxidative stress has also been shown to induce cell death by apoptosis, a programmed form of cell death (Kannan & Jain, 2000). Dying motor neurons in *Drosophila* and mouse models of ALS have been shown to express apoptotic markers, making increased oxidative stress as a result of a loss of SOD1 function one possible element of the disease mechanism (Xia et al., 2012; Guegan & Prezedborski, 2003).

Mitochondria have a place in the apoptotic pathway, through the release of proteins from the intermembrane space, and human ALS patients display aberrant mitochondrial morphology and distribution (Ott et al., 2007; Smith et al., 2017). In a mouse model of SOD1-mediated ALS, mitochondria in spinal cord motor neurons displayed more rounded and swollen morphology than the mitochondria of control mice (Vande Velde et al., 2011). The mitochondrial distribution in motor neurons of control mice was relatively homogenous, but the mitochondria in the ALS-model neurons were visibly aggregated in various regions of the cell (Vande Velde et al., 2011). A mouse model has also shown that axonal transport in motor neurons is impaired, which may contribute to abnormal mitochondrial distributions in the cell (Bilsland et al., 2010; De Vos et al., 2007). In addition to their key roles in apoptosis, oxidative homeostasis, and energy metabolism, mitochondria carry out essential regulations of calcium dynamics by uptaking or releasing calcium from the cytosol (Giorgi et al., 2018).

Mice carrying an ALS-linked allele of the SOD1 gene displayed attenuated calcium buffering capacity, possibly as a result of mitochondrial dysfunction (Beers et al., 2001). The possible effects of a loss of mitochondrial calcium sequestering ability extend to the broad array of physiological processes that employ calcium as an intracellular messenger. Regulation of calcium concentrations is crucial for synaptic transmission, and human patients with ALS display abnormal presynaptic physiology at motor synapses, with a selective loss of excitatory amino acid transporter 2 (EAAT2) (Lin et al., 1998). A loss of EAAT2 allows for increases in extracellular glutamate and overstimulation of glutamate receptors, which in turn could induce excitotoxic neurodegeneration (Zarei et al., 2015). Key factors in excitotoxicity include increases in oxidative stress and presynaptic calcium influx, both of which an organism with mutated SOD1 and dysfunctional mitochondria would have difficulty compensating for (Salińska et al., 2005). The finding revealing a loss of EAAT2 in ALS humans has been replicated in a mouse model (Trotti et al., 1999).

When *Sod* carries a missense mutation at or near structural Zn-binding sites, the SOD1 protein can misfold due to structural instability, forming aggregates as a result (Forsberg et al., 2011). The *Sod* alleles *G85R* and *H71Y*, examined in this study, are two such missense mutations. Some mutated forms of TDP-43 and FUS have also been shown to form aggregates, indicating that the formation of protein aggregates may be a shared mechanism for cases of ALS caused by mutations in a variety of genes (Chen & Cohen, 2019; Patel et al., 2015; Mackenzie & Rademakers, 2008). Mice carrying YFP-tagged transgenic ALS-related human alleles of SOD1 displayed motor paralysis phenotypes and died before reaching a year of age (Wang et al., 2008). Cells in sections of spinal cord from affected animals contained fluorescent punctae. Fractionation and gel filtration of spinal cord extracts revealed the presence of high molecular weight SOD1 multimers, heavier than either the SOD1 monomer or dimer alone, and protein sequencing of the SOD1-containing aggregates

181 revealed that they contained cytoskeletal proteins, including multiple species of
182 neurofilament, glial fibrillary acidic protein, and vimentin (Wang et al., 2008).
183
184 The fruit fly *Drosophila melanogaster* is a model organism with well-characterized physiology
185 and a fully sequenced genome (Adams et al., 2000). It is also a diploid organism with just
186 four pairs of chromosomes, including sex-linked X and Y chromosomes, allowing for
187 relatively easy genetic characterization. Due to its rapid lifecycle and the high number of
188 progeny each female produces, it is possible to generate datasets gathered from a large
189 number of rapidly-aging individuals, for example in studies of ALS. As a result, *Drosophila*
190 studies of ALS-related mutants can provide us with significant insight into physiological
191 variability between individual organisms in the context of the many heritable diseases that
192 express variably between human patients.
193
194 As a result of approx. 62% AA homology and the conservation of essential functional sites
195 between human and *Drosophila* SOD1, the *Drosophila Sod* alleles *G85R* and *H71Y*,
196 generated by ends-out homologous recombination, are homologous to mutations found in
197 human familial ALS-linked *Sod* alleles (Şahin et al., 2017). *G85R* and *H71Y* were generated
198 on the genetic background of w^{1118} (*white*), the white-eyed *Drosophila* mutant. In Sod^{G85R}, the
199 wild-type glycine residue at position 85 has been replaced with an arginine residue, and in
200 Sod^{H71Y}, the wild-type histidine residue at position 71 has been replaced with tyrosine. Both
201 mutation sites are in close proximity to metal ion binding sites that enable SOD1 to maintain
202 structural stability. Şahin et al. found that *Drosophila* homozygous for Sod^{G85R} and Sod^{H71Y}
203 displayed locomotor defects as larvae, pupal eclosion defects (full pupal lethality in Sod^{G85R}),
204 and short lifespans in Sod^{H71Y} adults. Sod^{H71Y} adults exhibited locomotor defects, along with
205 a loss of efferent branches in their leg neuromuscular junctions. In spite of this, no loss of
206 motor neuron cell bodies in the CNS was observed, suggesting that ALS-related

neurodegeneration at the synapse could precede death of motor neurons (Şahin et al., 2017).

Sod mutation-related neuromuscular defects may therefore also be observable at larval neuromuscular junctions (NMJs). The *Drosophila* larval fillet preparation, a live dissection method in which most internal organs are removed, and the muscle wall is laid bare, provides easy access to several repeating segments of stereotypically arranged NMJs for vital staining or electrophysiology-based investigations (Lee and Wu, 2010; Zhong et al. 1992; Ueda and Wu, 2006). The larval NMJ has well-documented morphology, which has been shown to display significant plasticity under the influence of genetic perturbations, including ion channel mutations and cAMP cascade dysregulation (Lee and Wu, 2010; Zhong et al., 1992). A readily accessible live NMJ is also ideal for imaging mitochondria made visible by staining, to investigate for distribution defects similar to those seen in a mouse ALS model (Vande Velde et al., 2011).

Materials and Methods

Fly stocks

Flies and larvae were housed in bottles containing a cornmeal-agar medium (Frankel & Brousseau, 1968). Flies were reared at a room temperature of 22 ± 1^{o}C. The *Sod* mutants examined were those of alleles *n108* (Phillips et al., 1989), *G85R*, and *H71Y* (Şahin et al. 2017). The wild-type control strain used for experiments without genetically encoded labels was Canton-S. For experiments in which a motor neuron membrane tag was needed, the stock used carried a chr. II UAS-CD8-GFP recombined with a chr. II motor neuron Gal4 driver (Brand & Perrimon, 1993), either C164-Gal4 (Torroja et al., 1999) or OK371-Gal4 (Mahr and Aberle, 2006). *Sod* lines used to produce the data represented in Figure 1 were balanced over a TM6 balancer with a dominant *Tubby* (*Tb*) marker.

Developmental lethality studies

Glass housing bottles used for these experiments contained cornmeal-agar medium, supplemented with 3g of yeast paste prepared as a 1:1 mixture of ddH_2O and active dry yeast (Red Star Yeast Co., LLC). Flies including 20-40 females were used to seed each bottle. Counts of deaths and eclosions were performed 16-17 d. after seeding.

Larval preparations, vital staining, & immunohistochemistry

Wandering third instar larvae were dissected, as per the "fillet preparation method", in HL 3.1 saline (Feng et al., 2004). All HL3.1 used in these experiments contained 0.1 mM Ca^{2+}. Tetramethylrhodamine (TMRM, $C_{25}H_{25}ClN_2O_7$) vital staining of larval preps for mitochondria was done at 100 nM in HL 3.1 for 20 minutes (in a light-impermeable chamber to prevent TMRM photobleaching), after which the bath was replaced with TMRM-free HL 3.1 before microscopy. Before antibody staining, larval preps were fixed in 3.7% formaldehyde in HL 3.1 for 25-30 minutes. Fixed preps were incubated with an FITC-conjugated goat antibody to HRP at 1:50 in phosphate buffer saline, at 4°C for 12-48 h. The antibody was obtained from Jackson ImmunoResearch Laboratories (West Grove, PA, USA). Anti-HRP recognizes a neural carbohydrate antigen in *Drosophila* (Kurosaka et al., 1991). Larval NMJ images, vital and fixed, were gathered on a Leica DM IL LED inverted microscope (Leica Microsystems Inc., Buffalo Grove, IL, USA), using the Leica Application Suite X software.

Larval NMJ morphology

NMJ boutons and branches were counted from muscles 4 (M4) and 13 (M13), in abdominal segments A3, A4, and A5. Counts from the three segments were pooled after no clear differences in the counts from different segments were found (data not shown). Counts of boutons from M4 include only type Ib boutons, and counts from M13 include both type Ib and

type Is. For branch counting, a branch was defined as a terminal process carrying at least two boutons (Zhong et al., 1992). An "enlarged terminal bouton" was defined as a bouton at the very end of a branch that was measurably larger than any other bouton on that branch, past the last branching point. This was often checked by holding a ruler up to the computer screen, to measure the width of the terminal bouton and nearby boutons, measured perpendicular to the directionality of the branch. "Elongated" boutons appear sausage-like, running down the branch past the point where a normal bouton would have narrowed to the "neck" that generally separates boutons. They had to also be of width equal to or greater than the widths of other boutons in the branch with the more common round morphology. If multiple elongated boutons appeared in a row, it could be difficult count them. In these cases, counts were conservative.

NMJ mitochondrial distributions

Imaging was completed within 30 minutes after TMRM staining to mitigate effects of post-dissection physiological decline on results. Boutons described as containing putative mitochondrial aggregates are those that stained strikingly more brightly than other boutons in the NMJ, and than the muscle staining in the background of the image. Fluorescence intensity was not computer-quantified, and so counts of terminal boutons that were especially brightly stained relied on the observer's judgement, but counts were conservative. Counts of putative mitochondrial aggregates in enlarged terminal boutons were obtained from larvae in which the NMJ membrane carried CD8-GFP driven by C164-Gal4 or OK371-Gal4, making bouton morphology visible in the green fluorescence channel during vital staining in the red channel.

285 Electrophysiology

286

287 All electrophysiological recordings were based on published protocols. Excitatory junction
288 potential recording (EJP) was adapted from Ueda and Wu, 2006 .Electrotonic stimulation
289 with tetrodoxin, 4-AP and TEA has been shown in Lee et al. (2014) for electrotonic
290 stimulation. Focal recording method was shown in (Ueda and Wu, 2012) and (Xing and Wu,
291 2018).

292

293 Statistics

294 Overall distributions of deaths throughout the lifecycle (Figure 1) were compared using
295 Fisher's exact test. Counts of NMJ boutons and branches and of enlarged terminal and
296 unsegregated boutons (Figures 2 and 4) were examined with Kruskal-Wallis testing between
297 all groups within muscle # and parameter (eg. M4, boutons), followed by rank-sum (Mann-
298 Whitney U) post hoc between individual groups. Distributions of counts of NMJ mitochondrial
299 aggregations of different categories (No aggregation, aggr. in terminal bouton, aggr. in
300 terminal + neighboring bouton) (Figure 3) were compared using Fisher's exact test.

301

302

303 **Results**

304

305 *Sod* developmental lethality

306 Wild-type produces no recorded wandering 3rd instar larval death, a low rate of pupal death
307 at ~3%, and no death during eclosion (Figure 1). In contrast, homozygotes from all three *Sod*
308 mutants display clear lethality during development. *n108* and *G85R* exhibited wandering 3rd
309 instar larval death rates of approx. 10% and 2%, respectively. The percent death rate refers
310 to a percentage of the total number of individuals counted at all stages. Only 4% of

311 individuals of the functionally-null *n108* allele died during the pupal stage. In the case of
312 individuals of the ALS-linked *G85R* allele, almost all pupae died before eclosion, though 1
313 out of 106 individuals made it into eclosion, before dying partway through the process,
314 leaving the room temperature *G85R* eclosion rate at 0. 44% of *n108* individuals died during
315 the eclosion process. The successful eclosion rates were 42% of *n108* and 43% of *H71Y*. No
316 dominant or semi-dominant *Sod* phenotype in the *Sod/TM6, Tb* individuals was apparent
317 during the stages of life leading up to eclosion. Like wild-type, none of them displayed larval
318 death or death at eclosion, and none had a pupal death rate above 4% (WT rate: 3%).
319
320 Larval neuromuscular junction morphology
321 When larvae were reared at room temperature, differences in neuromuscular junction
322 complexity between genotypes were mild in both muscles 4 (M4) and 13 (M13) (Figure 2).
323 Within genotypes, trends sometimes differed slightly the two muscles. M4 counts included
324 only type Ib bouton/branches, and M13 counts were from a combination of type Ib and type
325 Is boutons/branches, so small divergences in morphological quantifications between the two
326 muscles could reflect contributions from different bouton types. In M4, *n108* and *H71Y* both
327 displayed mean bouton numbers of approx. 17, compared to the mean of 14 in WT ($p <$
328 0.05). *G85R* M4 NMJs had on average 12 boutons, a non-significant decrease from WT.
329 Branch numbers exhibited the same relationships, but mean branch numbers for all
330 genotypes were between 2.3 and 2.8, with no statistically significant differences. Room
331 temperature M13 bouton and branch numbers showed mild decreases in *n108* and *G85R*
332 compared to WT, 13 boutons and 2.6 branches in *n108*, and 14 boutons ($p < 0.05$) and 2.6
333 branches in *G85R*, compared to 16 and 2.9 in WT.
334
335 The most notable NMJ morphology results were those concerning the morphology of
336 individual boutons. Depending on the allele and temperature conditioning, *Sod* mutants

displayed terminal boutons that appeared enlarged relative to other boutons on the same branch (Figure 4A), and thick, elongated boutons of morphology that could be described as "sausage-like" (Figure 4B). NMJs in WT reared at room temperature did occasionally carry boutons that fit the criteria (see methods) for these morphologies, but at low rates of about 0.5 enlarged terminal boutons and 0.3 elongated boutons per NMJ (Figure 4C). *n108* NMJs carried both bouton morphology types at higher rates than WT, approx. 0.9 of each type (compared to WT, enlarged $p < 0.05$, elongated $p < 0.001$) per NMJ. Enlarged terminal boutons appeared most frequently in *G85R* and *H71Y*, at rates of about 1.4 and 1.5 enlarged terminal boutons per NMJ ($p < 0.001$ in both genotypes), respectively. Elongated boutons in occurred at a rate of about 1.1 per NMJ ($p < 0.001$) in *G85R*. *H71Y* deviated from the trend a bit, producing elongated boutons only at a rate of ~0.6 per NMJ, which was less than *n108* and *G85R*, but still twice as much WT ($p < 0.05$).

Mitochondrial distributions at the larval NMJ

TMRM staining of the larval NMJ in Sod^{G85R} reared at RT revealed brightly stained, putative mitochondrial aggregations (Figure 3) in over half (55%) of all terminal boutons ($p < 0.001$), compared to just around 20% in WT (Figure 3). These apparent aggregations are in contrast to the more diffuse staining seen in most WT NMJs. Unlike *G85R*, the *n108* allele did not produce many mitochondrial aggregates in NMJ terminal boutons, in fact the rate was a little lower than WT, at 17%. Very interestingly, rearing the *G85R* larvae under heat stress actually appeared to provoke the disappearance of mitochondrial aggregations (drop to 14%, $p < 0.001$ for comparison to *G85R* RT), while in WT, heat stress prompted a mild increase in aggregates (~30% of terminal boutons), though this change was not statistically significant. *G85R* reared at RT and WT reared at HT, the two conditions under which the highest rates of terminal boutons containing aggregates appeared, also displayed the highest rates of immediately neighboring boutons carrying aggregates. In *G85R* RT, 29% of terminal boutons

363 containing aggregates were accompanied by neighbors also containing aggregates, and the
364 rate for WT HT was 33%. This is compared to 15% in WT RT, 14% in *G85R* RT, and 12% in
365 *n108* RT. If aggregation in both a terminal bouton and one or more neighbors represents a
366 more severe phenotype than aggregation in the terminal bouton alone, then more frequent
367 occurrences of the mitochondrial aggregation phenotype are accompanied by increased
368 severity of those occurrences.
369
370 In larvae carrying expressing GFP targeted to motor neuron membrane (UAS-CD8-GFP
371 under the control of OK371-Gal4 or C164-Gal4), an association between bouton morphology
372 and the presence of mitochondrial aggregates became apparent (Figure 5C). 83% of
373 enlarged terminal boutons in *G85R* reared at RT contained aggregates, compared to 55% of
374 terminal boutons of all morphologies. The aggregation-morphology relationship was also
375 present and conspicuous in wild-type: although only 15% of all terminal boutons contained
376 mitochondrial aggregates, 63% of terminal boutons that were enlarged contained
377 aggregates.
378
379
380 Mutants of sod and pk synergistically cause defects in synaptic transmission and excitability
381
382 Seeing the striking growth and structural defects in the synaptic terminals of *Sod* and *Pk*, we
383 would like to see if these phenotypes indicate any severe physiological symptoms. EJP
384 recording from postsynaptic muscle showed that *Sod* and Pk^{Pk} both exhibited enhanced
385 transmission compared to WT and Pk^{Sple} (Figure 5A and B). Most strikingly, the double
386 mutant of *Sod* and *Pk* synergistically enhanced the EJP amplitude, suggesting the
387 importance of *Sod* in *Pk*-mediated transport.

Additional analysis of the presynaptic terminal excitability was performed using electrotonic stimulation. NaV channels were all inhibited by TTX. Stimulation pulses were delivered at 1 ms duration instead of 0.1, and the stimulation electrode sucked the segmental nerve to nearly entry point into the muscle, so as to allow the stimulation to passively propagate to the synaptic terminals and depolarize the endplate membrane (Lee et al., 2014). In this way, CaV channels were directly triggered to open independent from NaV effects. Last but not least, a large portion of K+ channels were blocked by co-application of 4-AP and TEA. Such manipulations allow for the examination of terminal excitability fully driven by Ca2+ and potentially some less well-known K+ channels, with the axonal effects excluded. Using this method, we again observed that *Sod* and *Pk* mutants both generated gigantic plateau EJPs that could last more than 1 s, longer than those from WT. Although not in every case, double mutant of sod and pk sometimes even produced plateau EJPs that lasted more than 5 or 6 s. Similar results were obtained in the double mutant Pk^{Pk}/+ with Sod^{n108}, another allele of *Sod* mutant by focal recording (Fig 7). The focal recording results confirmed the dominant effects of pk allele, and indicated that the excitability defect was mainly in type Ib boutons (type Is not shown). All these results suggest a synergistic effect between sod and pk alleles in controlling the excitability of presynaptic terminals, which was governed by the local expression of Ca2+ and K+ channels.

Discussion

Developmental death in *Sod* mutants

The developmental data presented in this study deviate a bit from the results produced by Şahin et al., in that they reported a little under 30% successful eclosion for Sod^{H71Y}, as opposed to our rate of over 40%. One possibility is that the food supplementation with a large

amount of yeast (see methods) induced an increase in successful eclosion. In recent years, the Wu lab has been in the habit of adding chunks of yeast paste to the cornmeal-agar medium our *Sod* mutants are reared on, because it seems to improve the numbers and health of the mutant flies. Future experiments to clarify the basis and magnitude of this effect will naturally include more control experiments without yeast added, but also studies of *Sod* developmental health with the addition of yeast extract or heat-killed yeast in the place of our standard active yeast. This substitution could give indications as to whether any yeast-feeding effect is due to activity of live yeast, for example in the microbiome of *Drosophila*, in which case live yeast would be necessary, or to a simple nutritional value provided by the yeast, in which case yeast extract or heat-killed yeast would be sufficient to induce an effect on developmental health.

Aberrant NMJ morphology and physiology

The way in which the *n108* allele operates in synergy with heat stress to produce overgrowth, but does not produce overgrowth alone, is somewhat reminiscent of *Drosophila* mutants for other genes. The hyperexcitable K^+ channels mutants *Shaker* and *ether-a-go-go* each produce morphologically unremarkable NMJs on their own, but induce overgrowth once expressed together in the same larvae (Zhong et al., 1992). NMJ overgrowth in the cAMP phosphodiesterase mutant *dunce* is also magnified by the combination of *dunce* with either *Shaker* or *ether-a-go-go* (Zhong et al., 1992). Studies of the genetic interactions (or lack thereof) between Sod^{n108} and any of these mutants will help us understand the mechanisms that underlie overgrowth in heat-stressed *n108,* as well as the roles of oxidative stress in K^+ channel activity and cAMP metabolism.

The neuromuscular junction is, of course, primarily a synaptic structure, but this study stops short of any examination of synaptic transmission in *Sod* mutants. However, current

observations from the Wu lab indicate that presynaptic failure to release neurotransmitter upon stimulation in *n108* and *G85R* larvae reared at room temperature is not significantly different from wild-type (Dr. Xiaomin Xing, unpublished observations). Similarly, it also appears that *n108* reared at room temp. displays excitatory junction potentials upon nerve stimulation that are not significantly different from those in WT (Dr. Atsushi Ueda, unpublished observations). Further information about NMJ function in *Sod* mutants can be extracted from the system with the use of antibody stains for synaptic machinery. In particular, the densities and distributions of presynaptic active zones (stained by an antibody to Bruchpilot) and postsynaptic glutamate receptors (stained with an antibody to one of the DGluRII subunits) (Lee & Wu, 2010), can give us information on not just the functionality of the entire NMJ, but also of individual boutons of specific morphologies, including the enlarged terminal boutons and elongated boutons documented in this study. Staining of the subsynaptic reticulum, using an antibody to Discs large, will give us further information on any way in which the postsynaptic area has adapted, or failed to adapt, to boutons of unusual morphology (Lee & Wu, 2010). Staining may also be the key understanding the structural basis of the *Sod*-linked enlarged terminal and elongated boutons. It is unclear whether they are built up with expanded cytoskeletal components, or simply inflated. A practical and systematic way to approach this issue is to stain for various cytoskeletal component, such as actin and tubulin, using fluorophore-conjugated phalloidin and antibody stains. If the boutons are inflated beyond an earlier developmental shape and size, it is possible that some cytoskeletal components will have been left behind in the original shape of the boutons, and some will have moved outwards with the membrane.

Mitochondrial aggregation, between systems and ages

The mitochondrial aggregates observed at the larval NMJ and in culture could be related to dysfunctional intracellular transport, which has previously been reported in SOD1-based models of ALS (Bilsland et al., 2010; De Vos et al., 2007). In the case of the NMJ, reduced retrograde transport and/or increased anterograde transport could trap mitochondria at the end of the NMJ. This could then mean the aggregates disappear in *G85R* reared at HT because conditioning under heat stress somehow facilitates intracellular transport. But it's unclear what implications this would have for the phenotype in culture. Mitochondrial aggregates do not seem to localize to the very ends of neurites the way they localize to the ends of NMJ branches. These questions would be easier to approach with more information about the physical nature of the so-called mitochondrial aggregates. Due to the mechanics of TMRM, which is pulled into mitochondria by membrane potential (Chowdhury et al., 2016), increased fluorescence intensities due to higher membrane potential or due to mitochondrial volume may not be distinguishable. A possible solution could be to employ an indicator that is not sensitive to mitochondrial membrane potential, such as the genetically encoded mitochondrial indicator mito-roGFP (Albrecht et al., 2011). On the other hand, by design, it has the feature of becoming brighter when oxidized. This could complicate its use as a control for TMRM, but the additional information it could provide us may prove invaluable. Alternatively, dihyrorhodamine 123 (DHR123) (Ueda & Wu, 2008) is also a mitochondrial indicator relying on oxidation, though of the three it is likely the least practical: like TMRM, it relies on membrane potential to get into the mitochondria. Like mito-roGFP, DHR123 fluorescence is a reporter of oxidation, but DHR123 is not necessarily oxidized at the mitochondria, but rather in the cytoplasm, and it can be oxidized by a wide range of reactive oxygen species.

So far, the most important piece of information we have from the culture system is that there exists an early age at which an *Sod*^{G85R} mitochondrial phenotype does not strongly reveal

itself compared to wild-type. In the case of cultured giant motor neurons, that age is 3 days, and the phenotype somehow appears in the 3 to 4 days following that. With the current data, we can't know if the same process occurs at the larval NMJ, because larval dissections are done at the 6-day time point, and dissections of larvae earlier than that are tremendously difficult due to their small size. However, larvae younger than wandering 3rd instar, the stage at which we dissect, are quite translucent, and it is possible to use a confocal microscope to simply image fluorescence through the cuticle (Zito et al., 1999). A requirement for this technique would be to use a genetically-encoded mitochondrial indicator, and we have one: mito-roGFP. Concurrently, we can use the aforementioned *Drosophila* lines that express GFP in the presynaptic membrane of NMJs to track the development of elongated boutons and enlarged terminal boutons. Finally, confocal microscopy may enable the imaging of smaller scale structures around or within the aggregates, be it in young or older larvae, or in culture. And so the key to continuing this line of research appears to be the proper application of higher-power microscopy, as well as the continued, comprehensive exploitation of the relationship between the larval NMJ and the culture system.

References

Adams MD, Celniker SE, Holt RA, Evans CA, Gocayne JD, ... Venter JC. (2000) The genome sequence of *Drosophila melanogaster*. *Science* 287: 2185-2195.

Aitken RJ, Krausz C. (2001) Oxidative stress, DNA damage, and the Y chromosome. *Reproduction* 122: 497-506.

Albrecht SC, Barata AG, Großhans J, Teleman AA, Dick TP. (2011) In vivo mapping of hydrogen peroxide and oxidize glutathione reveals chemical and regional specificity of redox homeostasis. *Cell Metabolism* 14: 819-829.

Ali S, Jain SK, Abdulla M, Athar M. (1996) Paraquat induced DNA damage by reactive oxygen species. *Biochemistry and Molecular Biology International* 39(1): 63-67.

Altan O, Pabuccuoglu A, Altan A, Konyalioglu S, Bayraktar H. (2003) Effect of heat stress on oxidative stress, lipid peroxidation, and some stress parameters in broilers. *British Poultry Science* 44(4): 545-550.

Ayala GX, Tapia R. (2003) Expression of heat shock protien 70 induced by 4-aminopyridine through glutamate-mediated excitotoxic stress in rat hippocampus in vivo. *Neuropharmacology* 45: 649-660.

Baek MK, Kim KO, Kwon HJ, Kim YW, Woo JH, Kim DY. (2016) Age-related changes in antioxidative enzyme capacity in tongue of Fischer 344 rats. *Clinical and Experimental Otorhinolaryngology* 9(4): 352-357.

Beers DR, Ho BK, Siklos L, Alexianu ME, Mosier DR, Mohamed AH, ... Appel SH. (2001) Parvalbumin overexpression alters immune-mediated increases in intracellular calcium, and delays disease onset in a transgenic model of familial amyotrophic lateral sclerosis. *Journal of Neurochemistry* 79: 499-509.

Berlett BS, Stadtman ER. (1997) Protein Oxidation in Aging, Disease, and Oxidative Stress. *The Journal of Biological Chemistry* 272(33): 20313-20316.

Bilsland LG, Sahai E, Kelly G, Golding M, Greensmith L, Schiavo G. (2010) Deficits in axonal transport precede ALS symptoms in vivo. *Proc Natl Acad Sci* 107(47): 20523-20528.

Block ML, Calderón-Garcidueñas L. (2009) Air pollution: mechanisms of neuroinflammation and CNS disease. *Trends in Neurosciences* 32(9): 506-516.

Brand AH, Perrimon N. (1993) Targeted gene expression as a means of altering cell fates and generating dominant phenotypes. *Development* 118:401-415.

Campbell SH, Hilliker AJ, Phillips JP. (1985) Cytogenetic analysis of the *cSOD* microregion in *Drosophila melanogaster*. *Genetics* 112: 205-215.

Chen Q, Vasquez EJ, Moghaddas S, Hoppel CL, Lesnefsky EJ. (2003) Production of reactive oxygen species by mitochondria. *The Journal of Biological Chemistry* 278(38): 36027-36031.

Chen Y, Cohen TJ. (2019) Aggregation of the nucleic acid– binding protein TDP-43 occurs via distinct routes that are coordinated with stress granule formation. *J Biol Chem* 294(10): 3696-3706.

Chowdhury SR, Djordjevic J, Albensi BC, Fernyhough P. (2016) Simultaneous evaluation of substrate-dependent oxygen consumption rates and mitochondrial membrane potential by TMRM and safranin in cortical mitochondria. *Biosci Rep* 36: e00286

Culotta & Daly. (2013) Manganese Complexes: Diverse Metabolic Routes to Oxidative Stress Resistance in Prokaryotes and Yeast. *Antioxidants and Redox Signaling* 19(9): 933-944.

De Vos KJ, Chapman AL, Tennant ME, Manser C, Tudor EL, ... Grierson AJ. (2007) Familial amyotrophic lateral sclerosis-linked SOD1 mutants perturb fast axonal transport to reduce axonal mitochondria content. *Hum Mol Genet* 16(22): 2720-2728.

Dhalla NS, Temsah RM, Netticadan, T. (2000) Role of oxidative stress in cardiovascular diseases. *Journal of Hypertension*, 18(6): 655-673.

Feng, Y., Ueda, A., & Wu, C.-F. (2004). A modified minimal hemolymph-like solution, HL3. 1, for physiological recordings at the neuromuscular junctions of normal and mutant Drosophila larvae. *Journal of Neurogenetics*, 18(2): 377-402.

Forsberg K, Andersen PM, Marklund SL, Brannstrom T. (2011) Glial nuclear aggregates of superoxide dismutase-1 are regularly present in patients with amyotrophic lateral sclerosis. *Acta Neuropathol* 121: 623-634.

566 Frankel, A., & Brousseau, G. (1968). Drosophila medium that does not require dried yeast.
567 *Drosophila Information Service* 43, 184.
568 Galvin (2017) The path to specialist multidisciplinary care in amyotrophic lateral sclerosis: A
569 population- based study of consultations, interventions and costs. *PLoS ONE* 12(6):
570 e0178796.
571 Guegan S, Prezedborski C. (2003) Programmed cell death in amyotrophic lateral sclerosis. *J*
572 *Clin Invest* 111:153-161.
573 Giorgi C, Marchi S, Pinton P. (2018) The machineries, regulation and cellular functions of
574 mitochondrial calcium. *Nature Reviews: Molecular Cell Biology* 19: 713-730.
575 Hardiman O, van den Berg LH, Kiernan MC. (2011) Clinical diagnosis and management of
576 amyotrophic lateral sclerosis. *Nature Reviews: Neurology* 7: 639-649.
577 Kannan K, Jain SK. (2000) Oxidative stress and apoptosis. *Pathophysiology* 7(27) 153-163.
578 Kurosaka A, Yano A, Itoh N, Kuroda Y, Nakagawa T, Kawasaki T. (1991) The structure of a
579 neural specific carbohydrate epitope of horseradish peroxidase antiserum. *the*
580 *Journal of Biological Chemistry* 266(7): 4168-4172.
581 Landis G, Shen J, Tower J. (2012) Gene expression changes in response to again compared
582 to heat stress, oxidative stress and ionizing radiation in *Drosophila melanogaster*.
583 *Aging* 4(11): 768-789.
584 Lee J, Wu CF. (2010) Orchestration of Stepwise Synaptic Growth by K+ and Ca2+ Channels
585 in *Drosophila*. *J. Neurosci.* 30(47): 15921-15833.
586 Lee J, Ueda A, Wu CF (2014) Distinct roles of *Drosophila cacophony* and *Dmca1D* Ca2+
587 channels in synaptic homeostasis: Genetic interactions with *slowpoke* Ca2+-
588 activated BK channels in presynaptic excitability and postsynaptic response. *Dev.*
589 *Neurobiol.* 141: 4548-4557.
590 Liguori I, Russo G, Curcio F, Bulli G, Aran L, Della-Morte D, Gargiulo G, ... Abete P. (2018)
591 Oxidative stress, aging, and diseases. *Clinical interventions in Aging* 13: 757-772.

592 Lin CLG, Bristol LA, Jin L, Dykes-Hoberg M, Crawford T, Clawson L, Rothstein JD. (1998)
593 Aberrant RNA processing in a neurodegenerative disease: the cause for absent
594 EAAT2, a glutamate transporter, in amyotrophic lateral sclerosis. *Neuron* 20: 589-
595 602.
596 Lushchak, V. I. (2014). Free radicals, reactive oxygen species, oxidative stress and its
597 classification. *Chem-Biol Interact* 224: 164–175.
598 Mackenzie IRA, Rademakers R. (2008) Aberrant RNA processing in a neurodegenerative
599 disease: the cause for absent EAAT2, a glutamate transporter, in amyotrophic
600 lateral sclerosis. *Curr Opin Neurol* 21(6): 693-700.
601 Mahr A, Aberle H. (2006) The expression pattern of the *Drosophila* vesicular glutamate
602 transporter: A marker protein for motoneurons and glutamatergic centers in the
603 brain. *Gene Expression Patterns* 6: 299-309.
604 Massaad CA, Klann E. (2011) Reactive Oxygen Species in the Regulation of Synaptic
605 Plasticity and Memory. *Antioxidants and Redox Signaling* 14(10): 2013-2054.
606 Mates, J. M., Perez-Gomez, C., de Castro, IN. (1999). Antioxidant enzymes and human
607 diseases. *Clinical Biochemistry* 32(8): 595-603.
608 Mondola P, Damiano S, Sasso A, Santillo M. (2016) The Cu,Zn superoxide dismutase: not
609 only a dismutase enzyme. *Front Physiol* 7: 594.
610 Osking Z, Ayers JI, Hildebrandt R, Skruber K, Brown H, Ryu D, ... Vitriol EA. (2019) ALS-
611 linked SOD1 mutants enhance neurite outgrowth and branching in adult motor
612 neurons. *iScience* 11: 294-304.
613 Ott M, Gogvadze V, Orrenius S, Zhivotozsky B. (2007) Mitochondria, oxidative stress and
614 cell death. *Apoptosis* 12: 913-922.
615 Phillips JP, Campbell SD, Michaud D, Charbonneau M, Hilliker, AJ. (1989). Null mutation of
616 copper/zinc superoxide dismutase in Drosophila confers hypersensitivity to paraquat
617 and reduced longevity. *Proc Natl Acad Sci* 86(8): 2761-2765.

618 Patel A, Lee HO, Jawerth L, Maharana S, Jahnel M, Hein MY, Stoynov S, ... Alberti S. (2015)
619 A liquid-to-solid phase transition of the ALS protein FUS accelerated by disease
620 mutation. *Cell* 162, 1066-1077.
621 Peng IF, Berke BA, Zhu Y, Lee WH, Chen W, Wu CF. (2007) Temperature-dependent
622 developmental plasticity of *Drosophila* neurons: Cell-autonomous roles of
623 membrane excitability, Ca2+ influx, and cAMP signaling. *The Journal of*
624 *Neuroscience* 27(46): 12611-12622.
625 Perry JJP, Shin DS, Getzoff ED, Tainer JA. (2010) The structural biochemistry of the
626 superoxide dismutases. *Biochim Biophys Acta* 1804(2): 245-262.
627 Rosen DR, Siddique T, Patterson D, Figlewicz DA, Sapp P, Hentati A, ... Brown RH Jr.
628 (1993) Mutations in Cu/Zn superoxide dismutase gene are associated with familial
629 amyotrophic lateral sclerosis. *Nature* 362: 59-62.
630 Rowland LP, Shneider NA. (2001). Amyotrophic lateral sclerosis. *The New England Journal*
631 *of Medicine* 344(22): 1688-1700.
632 Ruan, H., & Wu, C. F. (2008). Social interaction-mediated lifespan extension of *Drosophila*
633 Cu/Zn superoxide dismutase mutants. *Proc Natl Acad Sci* 105(21): 7506-7510.
634 Saccon RA, Bunton-Stasyshyn RKA, Fisher EMC, Fratta P. (2013) Is SOD1 loss of function
635 involved in amyotrophic lateral sclerosis. *Brain* 136: 2342-2358.
636 Şahin A, Held A, Bredvik K, Major P, Achilli TM, Kerson, AG, ... Reenan, R. (2017). Human
637 SOD1 ALS mutations in a *Drosophila* knock-in model cause severe phenotypes and
638 reveal dosage-sensitive gain- and loss-of-function components. *Genetics* 205(2):
639 707-723.
640 Salińska E, Danysz W, Łazarexicz JW. (2005) The role of excitotoxicity in
641 neurodegeneration. *Folia Neuropathol* 43(4): 322-339.

642 Sies H. (1997) Oxidative Stress: Oxidants and Antioxidants (Physiological Society
643 Symposium: Impaired endothelial and smooth muscle cell function in oxidative
644 stress). *Experimental Physiology* 82: 291-295.
645 Smith EF, Shaw PJ, De Vos KJ. (2017) The role of mitochondria in amyotrophic lateral
646 sclerosis. *Neurosci Lett* 710: 132933.
647 Sørensen JG, Nielsen MM, Kruhøffer M, Justesen J, Loeschcke V. (2005) Full genome gene
648 expression analysis of the heat stress response in *Drosophila melanogaster*. *Cell*
649 *Stress Chaperones*. 10(4): 312-328.
650 Sosa V, Moliné T, Somoza R, Paciucci R, Kondoh H, Lleonart ME. (2013) Oxidative stress
651 and cancer: An overview. *Ageing Research Reviews* 12: 376-390.
652 Tang H, Tian E, Liu C, Wang Q, Deng H. (2013) Oxidative stress induces monocyte necrosis
653 with enrichment of cell-bound albumin and overexpression of endoplasmic reticulum
654 and mitochondrial chaperones. *PLoS ONE* 8(3): e59610.
655 Thannickal VJ, Fanburg BL. (2000) Reactive oxygen species in cell signaling. *Am J Physiol*
656 *Lung Cell Mol Physiol* 279: L1005-L1028.
657 Torroja L, Packard M, Gorczyca M, White K, Budnik V. (1999) The *Drosophila* β-amyloid
658 precursor protein homolog promotes synapse differentiation at the neuromuscular
659 junction. *The Journal of Neuroscience* 19(18): 7793-7803.
660 Trotti D, Rolfs A, Danbolt NC, Brown RH Jr, Hediger MA. (1999) SOD1 mutants linked to
661 amyotrophic lateral sclerosis selectively inactivate a glial glutamate transporter.
662 *Nature Neuroscience* 2(5): 427-433.
663 Tsang CK, Liu Y, Thomas J, Zhang Y, Zheng XFS. (2015) Superoxide dismutase 1 acts as a
664 nuclear transcription factor to regulate oxidative stress resistance. *Nat Commun*
665 5:3446.

Ueda A, Wu CF. (2006) Distinct frequency-dependent regulation of nerve terminal excitability and synaptic transmission by I_A and I_K potassium channels revealed by *Drosophila Shaker* and *Shab* mutations. *The Journal of Neuroscience* 26(23): 6238-6248.

Ueda A, Wu CF. (2008) Effects of *Hyperkinetic*, a beta-subunit of *Shaker* voltage- dependent K+ channels, on the oxidation state of presynaptic nerve terminals. *J Neurogenet* 22(2): 1-13.

Uttara B, Singh AV, Zamboni P, Mahajan RT. (2009) Oxidative stress and neurodegenerative diseases: a review of upstream and downstream antioxidant therapeutic options. *Current Neuropharmacology* 7: 65-74.

Van Raamsdonk JM, Hekimi S. (2012) Superoxide dismutase is dispensable for normal animal lifespan. *Proc Natl Acad Sci* 109(15): 5785-5790.

Vande Velde C, McDonald KK, Boukhedimi Y, ... Cleveland DW. (2011) Misfolded SOD1 Associated with Motor Neuron Mitochondria Alters Mitochondrial Shape and Distribution Prior to Clinical Onset. *PLoS ONE* 6(7): e22031.

Wang J, Farr GW, Zeiss CJ, Rodriguez-Gil DJ, Wilson JH, ... Horwich AL. (2008) Progressive aggregation despite chaperone associations of a mutant SOD1-YFP in transgenic mice that develop ALS. *Proc Natl Acad Sci* 106(5): 1392-1897.

Wang J, Farr GW, Hall DH, Li F, Furtak K, Dreier L, ... Horwich AL. (2009) An ALS-Linked Mutant SOD1 Produces a Locomotor Defect Associated with Aggregation and Synaptic Dysfunction When Expressed in Neurons of Caenorhabditis elegans. *PLoS Genetics* 5(1): e1000350.

Wang JW, Humphreys JM, Phillips JP, Hilliker AJ, Wu CF. (2000) A novel leg-shaking *Drosophila* mutant defective in a voltage-gated K^+ current and hypersensitive to reactive oxygen species. *Journal of Neuroscience* 20(16): 5958-5964.

690 Wu CF, Sakai K, Saito M, Hotta Y. (1990) Giant *Drosophila* neurons differentiated from
691 cytokinesis-arrested embryonic neuroblasts. *Journal of Neurobiology* 21(3): 499-
692 507.
693 Xia R, Liu Y, Yang L, Gal J, Zhu H, Jia J. (2012) Motor neuron apoptosis and neuromuscular
694 junction perturbation are prominent features in a *Drosophila* model of Fus-mediated
695 ALS. *Molecular Neurodegeneration* 7:10.
696 Zarei S, Carr K, Reiley L, Diaz K, Guerra O, Fernandez Altamirano P, ... Chinea A. (2015) A
697 comprehensive review of amyotrophic lateral sclerosis. *Surgical Neurology*
698 *International* 6:171.
699 Zhang Y, Liu Y, Walsh M, Bokov A, Ikeno Y, Jang YC, Perez VI, ... Richardson A. (2016)
700 Liver specific expression of Cu/ZnSOD extends the lifespan of *Sod1* null mice. *Mech*
701 *Ageing Dev* 154:1-8.
702 Zhong Y, Budnik V, Wu CF. (1992) Synaptic plasticity in *Drosophila* memory and
703 hyperexcitable mutants: role of cAMP cascade. *J Neurosci* 12(2): 644-651.
704 Zhong Y, Wu CF. (1991) Altered synaptic plasticity in Drosophila memory mutants with a
705 defective cyclic AMP cascade. *Science* 251(4990): 198-201.

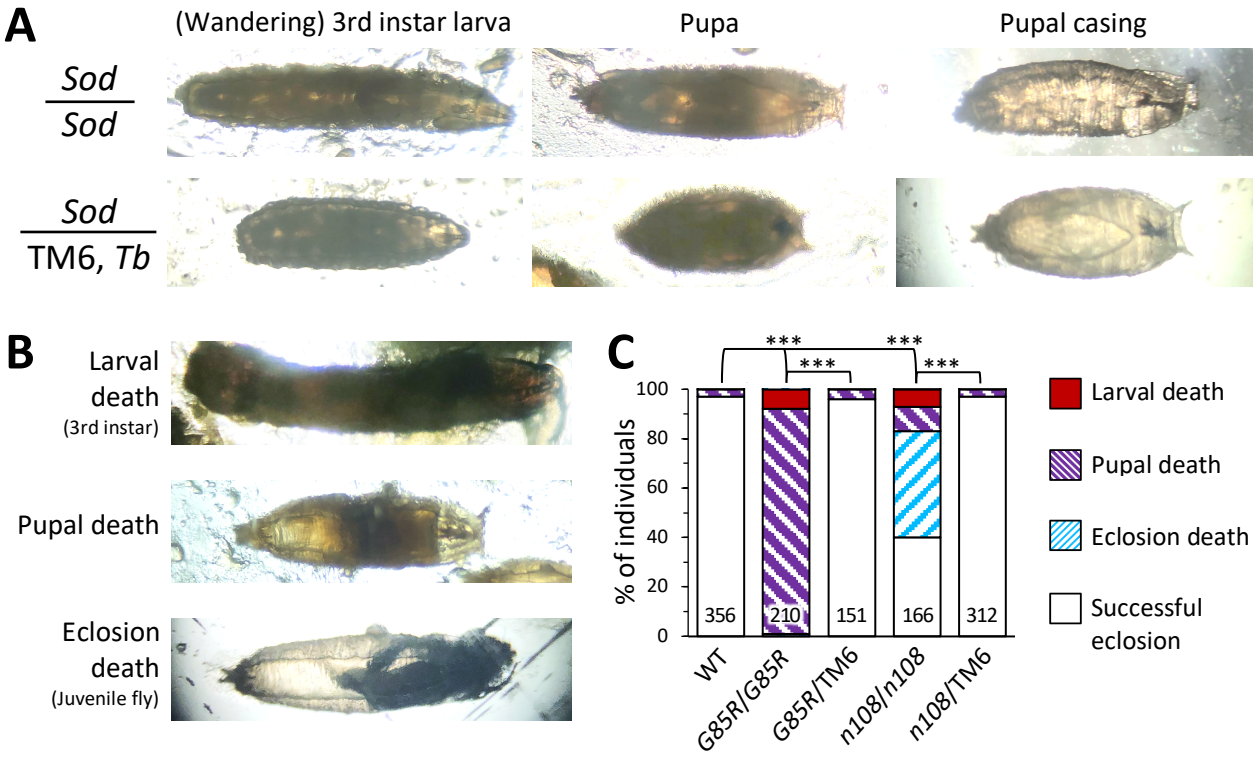

Figure 1. Developmental lethality in *Sod* mutants.

(A) Representative images of larvae, pupae, and empty pupal casings of *Sod* mutant homozygotes (*Sod*/*Sod*) and balanced heterozygotes (*Sod*/TM6, *Tb*). *Sod* homozygotes have wild-type body morphology, and the TM6 balancer granted the heterozygotes shorter and fatter *Tubby* (*Tb*) body shape. The larvae represented are specifically of the wandering 3rd instar stage, immediately pre-pupation. The empty pupal casing are left over after successful eclosion of the juvenile fly.

(B) Images of *Sod* homozygotes dead during the wandering 3rd instar larval, pupal, or eclosion stages. Dead larvae are identifiable by their immobility and dark color and dead pupae have unevenly distributed contents and dark patches. Juvenile flies dead during eclosion were distinguished from flies in the process of eclosing by a second observation 15-30 min after the first. Juvenile fly corpses were also frequently darker than their live counterparts.

(C) Rates of lethality during development in wild-type (WT), Sod^{G85R} (*G85R*/*G85R*), Sod^{G85R}/TM6,*Tb* (*G85R*/TM6), Sod^{n108} (*n108*/ *n108*), and Sod^{n108}/TM6,*Tb* (*n108*/TM6). Dead individuals were counted at the 3rd instar larval stage (red), pupal stage (purple), and eclosion (blue). Rates of successful eclosions (white) are from counts of empty pupal casings. *** indicates $p < 0.001$ (Fisher's exact test). *n* of individuals are indicated at the bottom of each bar.

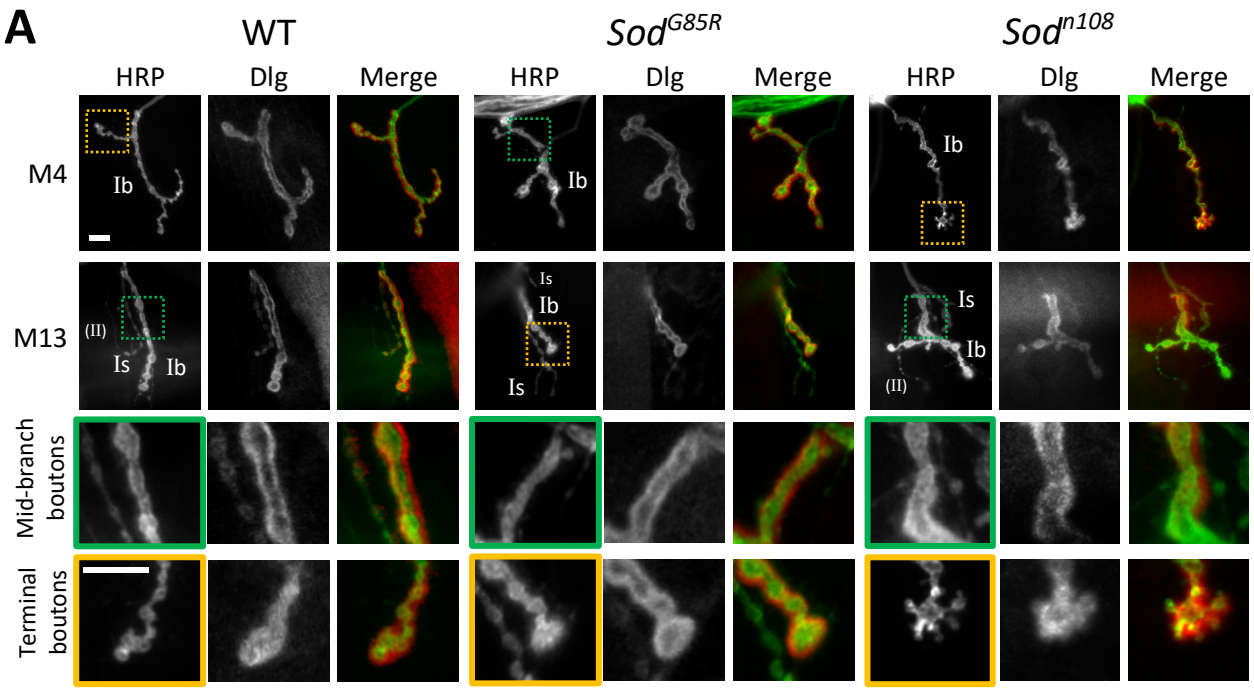

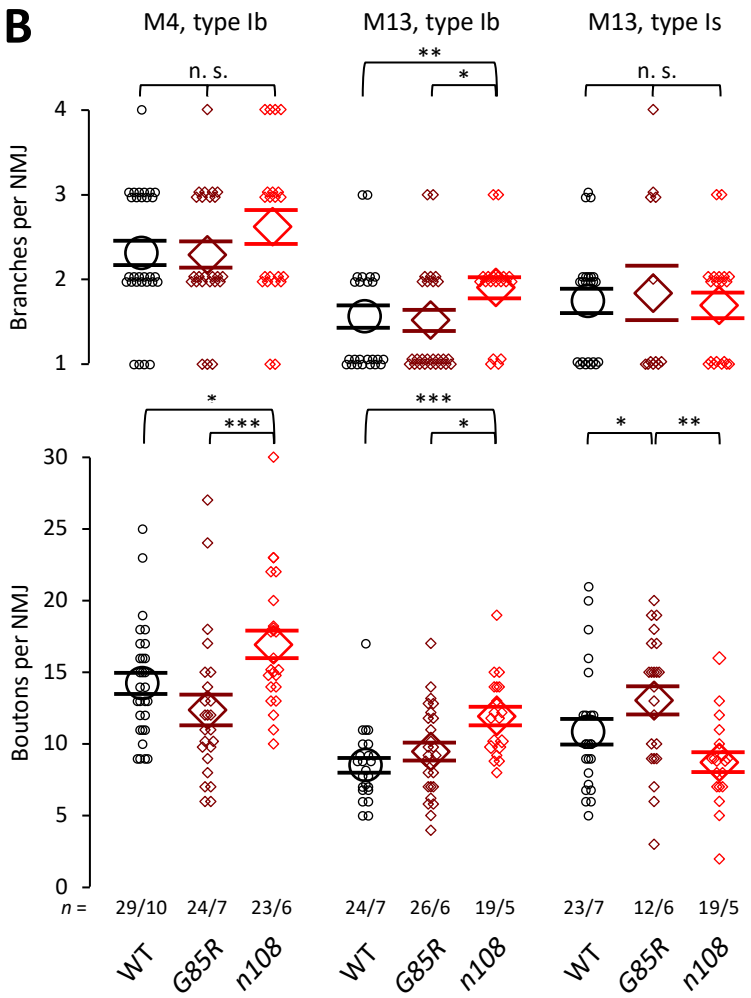

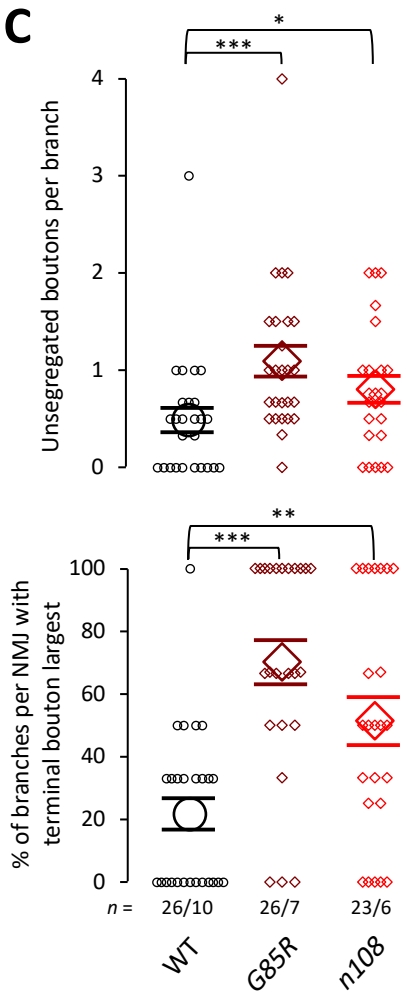

Figure 2. Morphological defects in larval motor synapses of *Sod* mutants.

(A) Representative NMJ of larval muscles 4 (M4) and 13 (M13) from WT, Sod^{G85R}, and Sod^{n108}, immunostained with anti-HRP (neuronal membrane, green in merged image) and anti-Dlg (subsynaptic reticulum, red in merged image). Type Ib (tonic glutamatergic) branches were examined in both muscles, and type Is (phasic glutamatergic) branches were examined in M13. Is branches are distinguishable from Ib by their smaller size , and weaker anti-HRP and anti-Dlg immunostaining. Labels on the anti-HRP images indicate branch types. The much smaller type II boutons are also labeled, but were not studied. Select portions of the M4 and M13 images are magnified to show phenotypic incomplete bouton segregation (third row, green boxes) and terminal bouton enlargement (fourth row, gold boxes) in Sod^{G85R} and Sod^{n108}, compared to common WT variation. Note the "satellite" buds present on the magnified terminal bouton from Sod^{n108}. Scale bars in the upper left and lower left images are 10 µm.

(B) Per NMJ, number of branches (top) and synaptic boutons (bottom) of type Ib in M4 and M13, and type Is in M13. Branches are defined here as terminal processes composed of two or more synaptic boutons, distal of any bifurcations. Counts from larval abdominal segments 3, 4, and 5 are pooled. WT counts are plotted as black circles, Sod^{G85R} (*G85R*) as maroon diamonds, Sod^{n108} (*n108*) as red diamonds. Means are indicated by enlarged symbols, SEM by bars. * indicates $p < 0.05$, ** indicates $p < 0.01$, *** indicates $p < 0.001$ (Kruskal-Wallis test, rank-sum post hoc). *n* numbers (*n* of NMJ/*n* of larvae) are indicated above the genotype labels.

(C) Number of incompletely segregated (unsegregated) boutons per Ib branch per M4 NMJ (top), and percentage of Ib branches per M4 NMJ in which the terminal bouton was the largest after the last bifurcation. A bouton was described as incompletely segregated if the width of the narrowest point on the neck preceding it was greater than 80% of the width of the widest point on the bouton. The statistical parameters and their layout are identical to those of panel B.

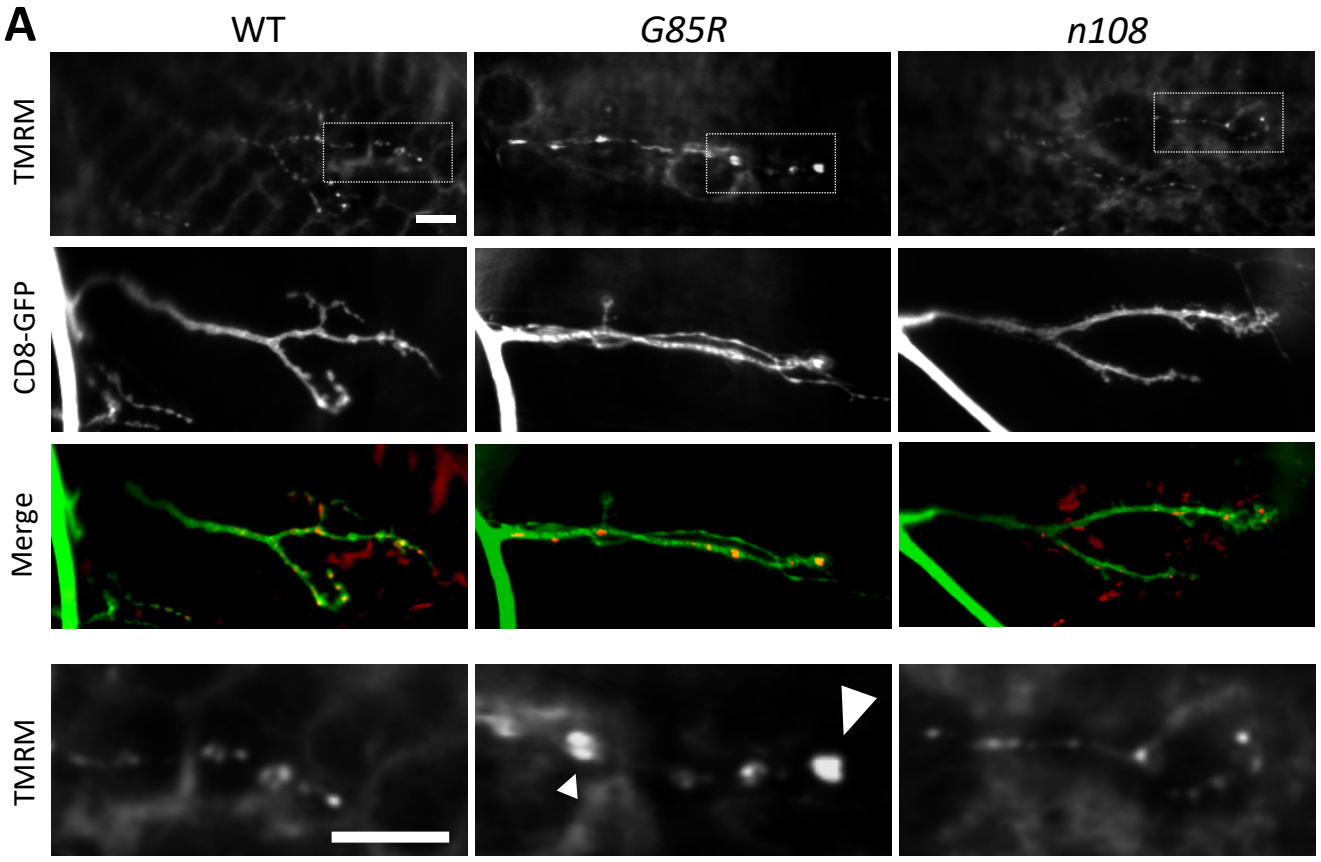

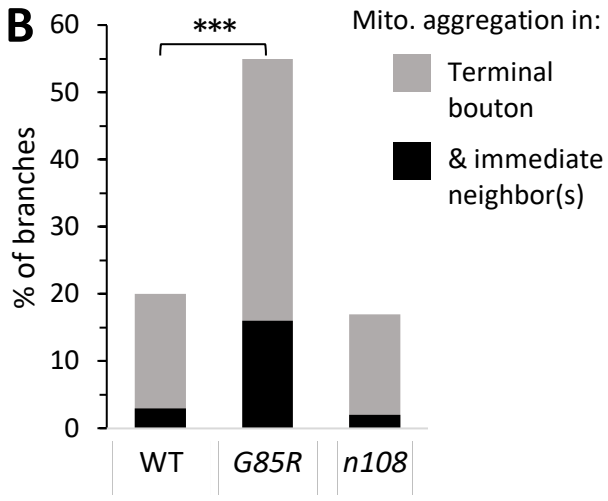

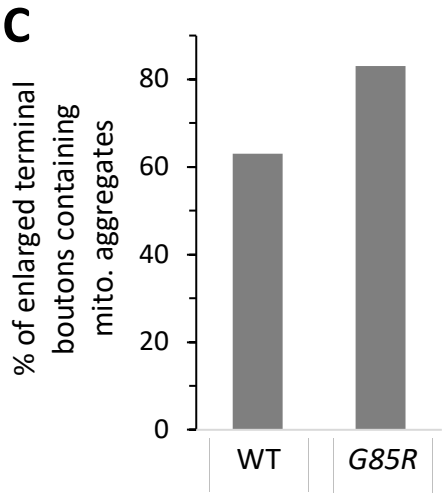

Figure 3. Putative mitochondrial aggregates in terminal NMJ boutons of *Sod*^{G85R} larvae, frequently present in enlarged terminal boutons.

(A) Mitochondrial live tissue staining (TMRM, first row) in muscle 4 NMJ terminal branches in wild-type (left), *Sod*^{G85R} (center), and *Sod*^{n108} (right) larvae. Second row is NMJ morphology, visible with a presynaptic membrane-targeted GFP (CD8-GFP), expression of which was driven by a Gal4 construct (C164 or OK371). Third row is an overlay of the first and second row. Fourth row contains magnified portions of the whole-NMJ TMRM images (first row, white boxes). Large white arrowhead indicates a brightly-stained potential aggregation of mitochondrial in the *Sod*^{G85R} terminal bouton, smaller white arrowhead indicates bright mitochondrial staining in a non-terminal bouton. Scale bars in the upper left and lower left images are 10 μm.

(B) Percentages of branches in which putative mitochondrial aggregates appear in the terminal bouton (gray), or in the terminal bouton and one or more immediate neighbors (black), in WT, *Sod*^{G85R}, and *Sod*^{n108}. For WT vs *Sod*, *** indicates $p < 0.001$ (Fisher's exact test, comparing distributions of counts of terminal boutons without mito. aggr., with mito. aggr., and of terminal + neighboring bouton(s) with mito. aggr..).

(C) Percentages of terminal boutons with enlarged morphology (visible with CD8-GFP) in which putative mitochondrial aggregation appears, in WT and *Sod*^{G85R} larvae. Includes counts from NMJs of muscles 4, 6, 7, 12, 13 in segments A2 through A6. *n* of branches/NMJs/larvae: WT = 93/35/3, *G85R* = 174/76/5, , *n108* = 53/27/3.

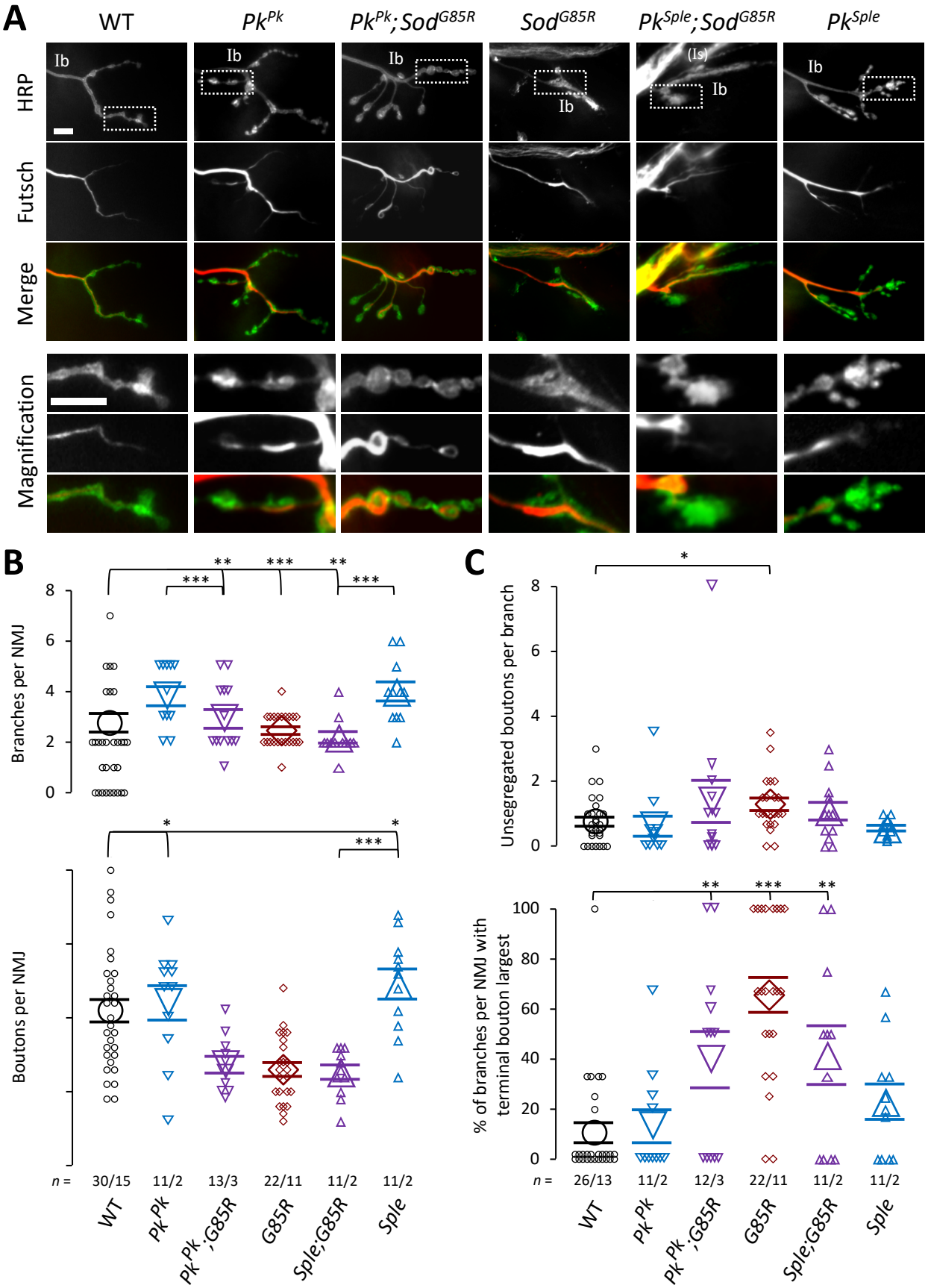

Figure 4.

(A) Representative NMJ of larval muscle 4 (M4) (Ib branches) from WT, Sod^{G85R}, Pk^{Pk}, Pk^{Sple}, and the double mutants Pk^{Pk};Sod^{G85R} and Pk^{Sple};Sod^{G85R}. Presynaptic neuronal membrane is immunostained with anti-HRP (green in merged image) and the microtubule-associated protein Futsch is stained with the monoclonal AB 22C10 (red in merged image). Is branches are labeled where appropriate, but were not studied here. Select portions of the full-scale images are magnified to show characteristic bouton morphologies and cytoskeletal structures (bottom three rows). Note the greater and irregular intensities of Futsch staining in Sod^{G85R}, Pk^{Pk}, and Pk^{Pk};Sod^{G85R}, and the strongly stained "loop" structures in Pk^{Pk};Sod^{G85R}. Scale bars in the full-scale and magnified HRP images are 10 µm.

(B) Per M4 NMJ, number of type Ib branches (top) and synaptic boutons (bottom). Counts from larval abdominal segments 2, 4, and 6 are pooled. WT counts are plotted as black circles, Pk^{Pk} as blue inverted triangles, Pk^{Pk};Sod^{G85R} (Pk^{Pk};*G85R*) as purple inverted triangles, Sod^{G85R} (*G85R*) as maroon diamonds, Pk^{Sple};Sod^{G85R} (*Sple*;*G85R*) as purple upright triangles, (*Sple*) as blue upright triangles. Means are indicated by enlarged symbols, SEM by bars. * indicates $p < 0.05$, ** indicates $p < 0.01$, *** indicates $p < 0.001$ (Kruskal-Wallis test, rank-sum post hoc). *n* numbers (*n* of NMJ/*n* of larvae) are indicated above the genotype labels.

(C) Number of incompletely segregated (unsegregated) boutons per Ib branch per M4 NMJ (top), and percentage of Ib branches per M4 NMJ in which the terminal bouton was the largest after the last bifurcation. A bouton was described as incompletely segregated if the width of the narrowest point on the neck preceding it was greater than 80% of the width of the widest point on the bouton. The statistical parameters and their layout are identical to those of panel B.

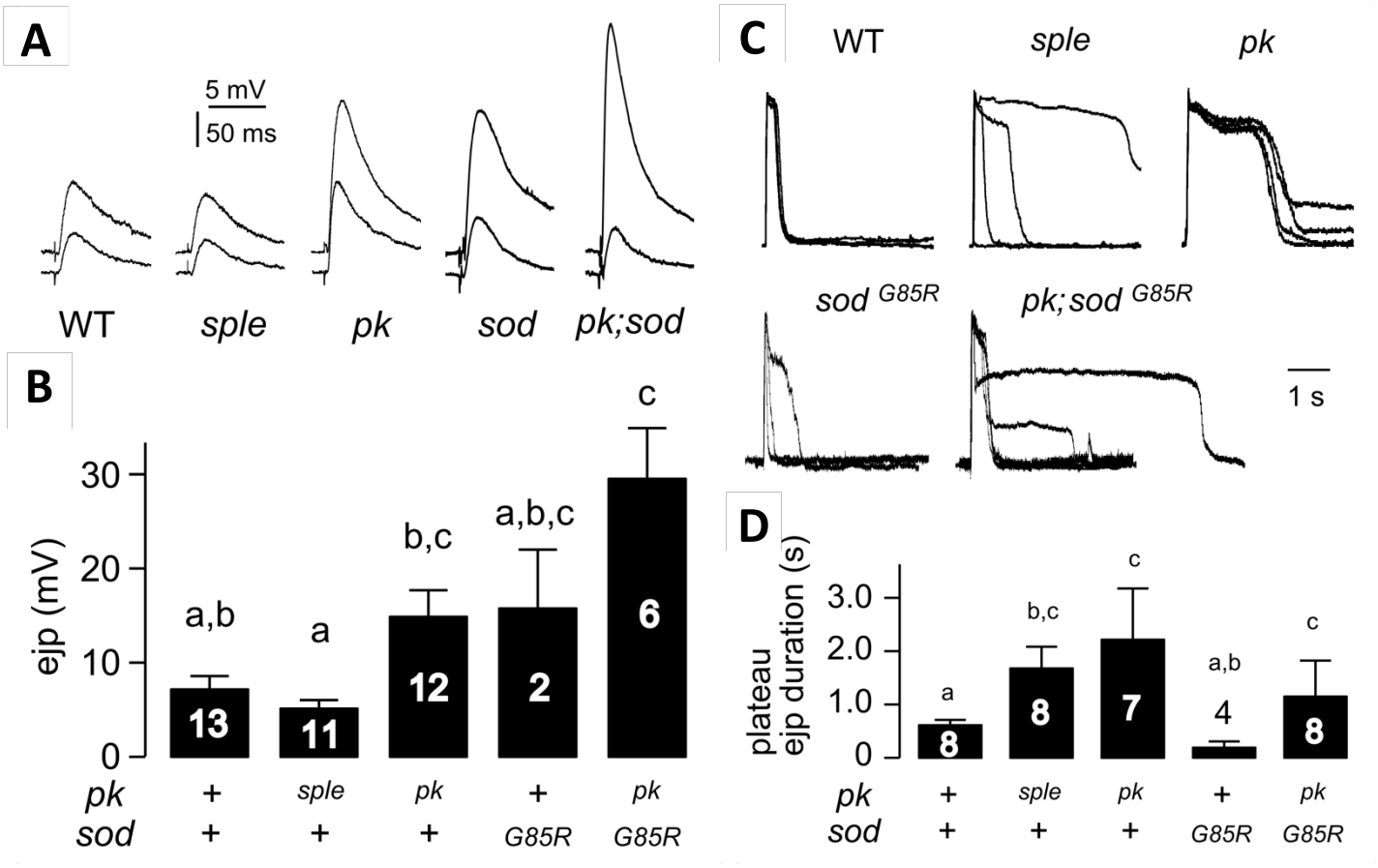

Figure 5.

(A) Increased size and variability of excitatory junctional potentials (ejps) from larval body wall muscles in *Pk* and *Pk;Sod*^{G85R}. Ejps from two different muscles are shown as examples for each genotype.

(B) a, b, and c indicates that differences within the group is not significant ($p > 0.05$, F-test). Error bars = SEM. Number of NMJs are indicated.

(C) Excitability in *Pk* and *Sod*^{G85R} motor axon terminals. Synaptic transmission was induced by direct activation of the motor axon terminals by electrotonic stimulation in the presence of a Na+ channel blocker (TTX, 3 µM) and K+ channel blockers (4-AP, 200 µM and TEA, 20 mM). Under this condition, prolonged ejps supported by continuous transmitter release were recorded (see Text). Amplitude is normalized to the peak.

(D) The duration of plateau ejps were prolonged and more variable among perparations in *Pk*^{Sple}, *Pk*^{Pk}, and *Pk*^{Pk};*Sod*^{G85R}. a, b, and c indicates that differences within the group is not significant ($p > 0.05$, F-test). Error bars = SEM. Number of NMJs are indicated.

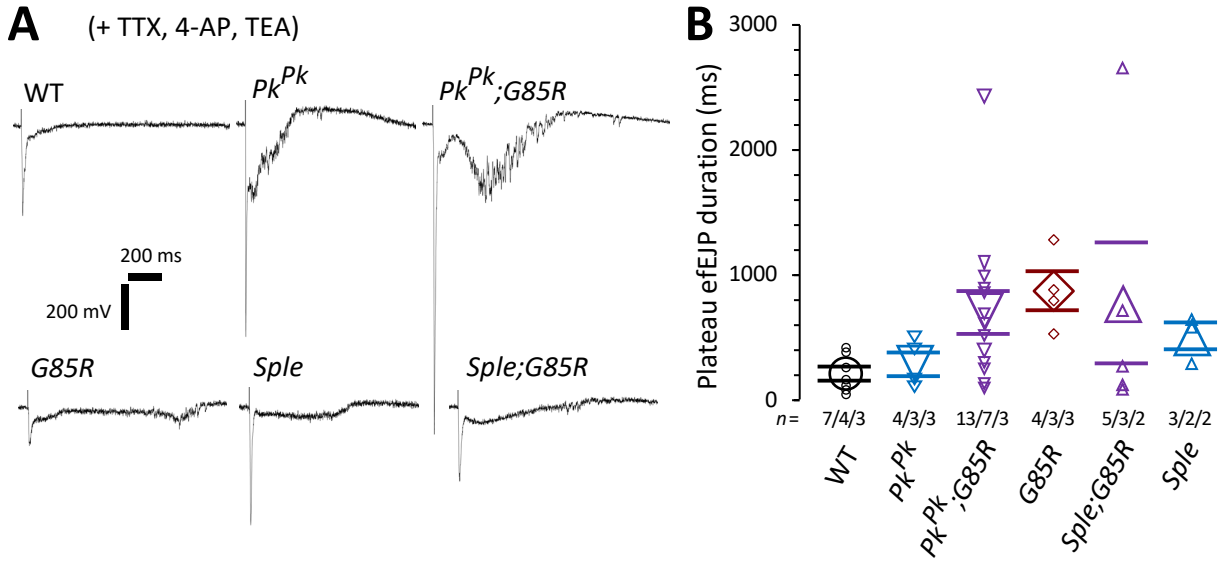

Figure 6. Focal recording of plateau-like potentials induced at neuromuscular synapses by K^+ channel blockers.

(A) Sample focal recording (efEJP) traces from neuromuscular synapses of WT, Sod^{G85R}, Pk^{Pk}, Pk^{Sple}, Pk^{Pk};Sod^{G85R}, and Pk^{Sple};Sod^{G85R}. , upon electrotonic stimulation after application of TTX (3 µM), 4-AP (200 µM), and TEA (20 mM). Recordings are from the NMJ of muscles 6 and 7, in larval segments A4 and A5. Each recording site contained between 1 and 4 boutons, and could contain a mixture of type Ib and type Is boutons. Note that trace amplitude is dependent on the variable seal resistance between the recording electrode and the NMJ. All artifacts have been truncated.

(B) Durations of plateau-like efEJP. At each recording site, a series of single stimulation pulses will incrementally increasing voltage was applied. The plotted plateau efEJP duration for each site is a measurement from the first plateau observed in the stimulation series. WT counts are plotted as black circles, Pk^{Pk} as blue inverted triangles, Pk^{Pk};Sod^{G85R} (Pk^{Pk};*G85R*) as purple inverted triangles, Sod^{G85R} (*G85R*) as maroon diamonds, Pk^{Sple};Sod^{G85R} (*Sple*;*G85R*) as purple upright triangles, (*Sple*) as blue upright triangles. Means are indicated by enlarged symbols, SEM by bars. *n* numbers (*n* of recording sites/*n* of NMJ/*n* of larvae) are indicated above the genotype labels.

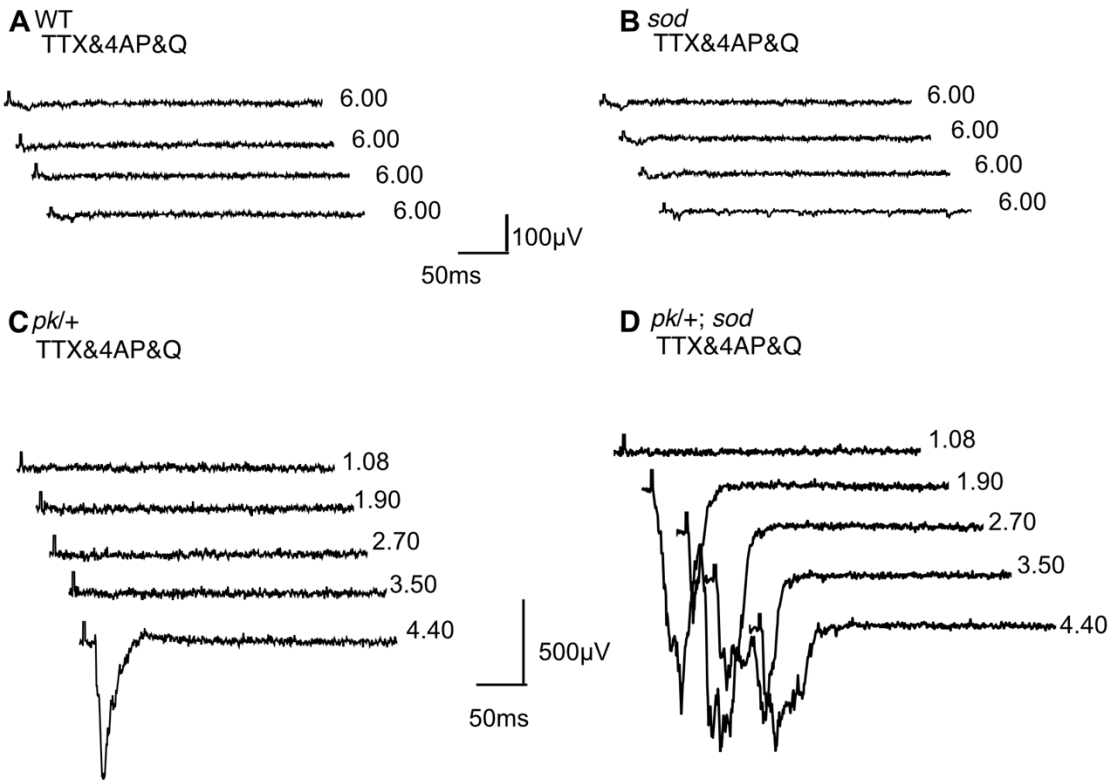

Figure 7. Focal recording examination of the excitability in *pk*^{pk} and *sod*^{n108} synaptic terminals.

Electrotonic stimuli (1 ms pulse duration) were applied to NMJ terminals at 0.1mM Ca2+ with Na^+ channel blockers (TTX, 3 µM) and K^+ channel blockers (4-AP, 200 µM and quinidine, 100 µM). Only type Ib boutons were recorded. (A) WT and (B) *sodn108* terminals quickly ran down after adding both 4-AP and quinidine and gave poor responses, whereas (C) *pk*^{pk} heterozygous (over CyO-GFP) and (D) *pk*^{pk}/CyO-GFP; *sodn108* displayed currents of striking amplitudes. Note that *pk*^{pk}/CyO-GFP; *sodn108* has lower stimulation voltage (in V, labeled on the side) threshold and wider response current width. All artifacts have been truncated.